

A survey for low mass spectroscopic binary stars in the young clusters around σ Orionis and λ Orionis.

P.F.L. Maxted¹, R.D. Jeffries¹, J.M. Oliveira¹, T. Naylor², R.J. Jackson¹

¹*Astrophysics Group, Keele University, Keele, Staffordshire ST5 5BG, United Kingdom*

²*School of Physics, University of Exeter, Stocker Road, Exeter, EX4 4QL*

Submitted 2007

ABSTRACT

We have obtained multi-epoch, high-resolution spectroscopy of 218 candidate low-mass stars and brown dwarfs in the young clusters around σ Ori and λ Ori. We find that 196 targets are cluster members based on their radial velocity, the equivalent width of their Na I 8200 lines and the spectral type from their TiO band strength. We have identified 11 new binary stars among the cluster members based on their variable radial velocity and an additional binary from the variation in its line width and shape. Of these, 6 are double-lined spectroscopic binaries (SB2) where the components of the binary are of comparable brightness. The others are single-lined binaries (SB1) in which the companion is faint or the spectra of the stars are blended. There are 3 narrow-lined SB1 binaries in our sample for which the companion is more than 2.5 magnitudes fainter than the primary. This suggests that the mass ratio distribution for the spectroscopic binaries in our sample is broad but that there may be a peak in the distribution near $q = 1$. The sample covers the magnitude range $I_C = 14 - 18.9$ (mass $\approx 0.55 - 0.03M_\odot$), but all of the binary stars are brighter than $I_C = 16.6$ (mass $\approx 0.12M_\odot$) and 10 are brighter than $I_C = 15.5$ (mass $\approx 0.23M_\odot$). There is a significant lack of spectroscopic binaries in our sample at faint magnitudes even when we account for the decrease in sensitivity with increasing magnitude. We can reject the hypothesis that the fraction of spectroscopic binaries is a uniform function of I_C magnitude with more than 99 percent confidence. The spectroscopic binary fraction for stars more massive than about $0.1M_\odot$ ($I_C < 16.9$) is $f_{\text{bright}} = 0.095^{+0.012}_{-0.028}$. The 90 percent confidence upper limit to the spectroscopic binary fraction for very low mass (VLM) stars (mass $< 0.1M_\odot$) and brown dwarfs (BDs) is $f_{\text{faint}} < 7.5$ percent. The hypothesis that f_{bright} and f_{faint} are equal can be rejected with 90 percent confidence. The average detection probability for our survey is 50 percent or more for binaries with separations up to 0.28 au for stars with $I_C < 16.9$ and 0.033 au for the fainter stars in our sample. We conclude that we have found strong evidence for a change in the fraction of spectroscopic binaries among young VLM stars and brown dwarfs when compared to more massive stars in the same star-forming region. This implies a difference in the total binary fraction between VLM stars and BDs compared to more massive stars or a difference in the distribution of semi-major axes, or both.

Key words: binaries: spectroscopic – stars: low-mass, brown dwarfs.

1 INTRODUCTION

The origins of very low-mass stars (VLMS) and brown dwarfs (BD) are proving difficult to understand, despite being more common than stars of higher mass. Ideas include ejection from protostellar aggregates (Reipurth & Clarke 2001), formation within convergent flows generated by turbulence (Padoan & Nordlund 2004), the photo-erosion of pre-stellar cores (Whitworth & Zinnecker 2004) or fragmentation within the outer parts of circumstellar discs (Whitworth & Stamatellos 2006).

The frequency and separation distribution of binary systems is an important constraint on the likely formation process. There is strong evidence that the binary properties of the lowest mass stars and brown dwarfs are quite different to those of higher mass objects (see the review of Burgasser et al. 2007). Resolved imaging of nearby VLMS and BDs in the field show that about 15–20 percent of systems are binaries with separations greater than 1–2 au, but that very few have separations greater than 20 au (e.g. Close et al. 2003; Bouy et al. 2003). This contrasts with

higher mass stars where overall binary frequencies are 30–60 percent, with a much broader spread of possible separations (Fischer & Marcy 1992, Duquennoy & Mayor 1991).

A missing part of the picture is how many VLMS and BDs are binary systems with separations less than about 1 au, where the imaging observations cannot reach. Maxted & Jeffries (2005) used previously published radial velocity (RV) results to show that an overall binary frequency (at all separations) of 32–45 percent was needed to explain the presence of several binaries detected by RV variations, with most of them at small separations. This high frequency found support from a small RV survey by Kurosawa et al. (2006) who found a frequency of 11–40 percent for separations less than 0.1 au in a young association. On the other hand Basri & Reiners (2006) found few RV variables in their survey of field VLMS/BDs and concluded that the overall binary frequency was 16–36 percent, with very few binaries at separations below 1 au.

The situation is unresolved and it is quite likely that the apparent discrepancies between these various authors arise from biases within the samples considered; differences in analysis technique and that in terms of absolute numbers, very few short-period VLMS/BD binary systems have yet been found, thus limiting the statistical precision possible.

In this paper we present the results of an RV survey of a large number of low-mass stars and brown dwarfs in the σ Ori and λ Ori clusters. These clusters are young and nearby (3–5 Myr, 330–450 pc) and contain large populations of VLMS and BDs (Béjar et al. 2004; Barrado y Navascués et al. 2004; Kenyon et al. 2005). We have observed more than 200 objects using the FLAMES multi-fibre spectrograph on the VLT-Kueyen telescope to measure radial velocities at several epochs and searched for close binary systems at a range of masses.

2 OBSERVATIONS AND DATA REDUCTION

2.1 Observations

We have used the FLAMES multi-object spectrograph (Pasquini et al. 2002) on ESO’s VLT UT2 (Kueyen) telescope to obtain multi-epoch, high-resolution spectroscopy of 218 faint stars in the clusters around σ Ori and λ Ori. The instrument is capable of providing spectra of up to 130 targets in one setting over a field of view 25 arcmin in diameter.

We selected targets around σ Ori from the photometric catalogue of Kenyon et al. (2005). We included all stars in the magnitude range $14 < I_C < 19$ with the correct I_C magnitude and $(R_C - I_C)$ colour to be a cluster member in the input catalogue for the fibre allocation process, irrespective of any other membership information that may have been available. For λ Ori all the candidate members identified in the catalogue of Barrado y Navascués et al. (2004) were included in the input catalogue for the fibre allocation process. Fibres were allocated in 6 fields, 2 fields near λ Ori and 4 fields near σ Ori. The central position of each field and the number of targets for which useful spectra were obtained are given in Table 1. The position of the targets in the I_C v. $(R_C - I_C)$ colour-magnitude diagram is shown in Fig. 1. Those fibres that could not be allocated to targets were used

Table 1. Log of observations. The number of stars observed with the GIRAFFE spectrograph on each date for which useful spectra (signal-to-noise ratio > 5) were obtained is given in the column headed N . The date of observation is given in the fifth column. The standard deviation of the radial velocities of the night sky emission line spectra obtained at each epoch, σ_{sky} , are given in the final column.

Field	Position		N	Date (UTC)	σ_{sky} (km s^{-1})
	α_{J2000}	δ_{J2000}			
λ Ori 1	05 35 58.5	+09 51 21	34	2005 10 14	0.66
			34	2005 11 17	0.59
			35	2005 12 30	0.67
λ Ori 2	05 34 44.1	+09 51 44	49	2005 10 14	0.64
			49	2005 11 27	0.99
			50	2005 11 28	0.63
			50	2005 12 30	0.58
σ Ori 1	05 40 28.0	−02 15 35	26	2005 11 13	0.60
			22	2005 11 17	0.60
			26	2006 01 08	0.64
			26	2006 01 13	0.92
σ Ori 2	05 40 01.6	−02 40 02	17	2005 11 13	0.67
			29	2005 12 07	0.65
			28	2006 01 13	0.74
σ Ori 3	05 38 26.9	−02 41 21	56	2005 11 13	0.64
			55	2005 11 24	0.67
			56	2005 12 07	0.56
			55	2006 01 13	0.60
σ Ori 4	05 38 23.8	−02 14 59	33	2005 11 11	0.59
			34	2005 11 11	0.58
			34	2005 12 07	0.62
			32	2006 01 13	0.60

to obtain simultaneous background spectra for sky subtraction. The two fields around λ Ori overlap so 10 stars were observed in 2 fields. For most stars we have obtained 3–4 spectra with the exception of 10 stars observed in 2 fields for which we typically have 6–7 spectra. The baseline of the observations is at least 24 days for all stars and is more typically 60–70 days. The sensitivity of our survey drops rapidly for binaries with semi-major axes $a \gtrsim 0.25$ au as a result of the baseline of our observations.

Light from the fibres was fed to the GIRAFFE spectrograph operated in a high resolution mode with the H836.6 echelle grating. A filter was used to select light from the 6th echelle order which covers the wavelength region 8073–8632Å. The resolving power of the spectra is $R \approx 16000$. Spectra were obtained in service mode by ESO staff on the dates given in Table 1. The exposure time in each case was 2750 s. The seeing during the exposures was typically 0.92 arcsec but varied from 0.48 arcsec to 1.45 arcsec.

We also took advantage of the possibility to use up to 8 fibres from FLAMES to obtain spectra with the UVES echelle spectrograph (Dekker et al. 2000) at the same time as the GIRAFFE observations. We used the CD#4 echelle grating to obtain spectra at a resolution of $R \approx 47000$ covering the same spectral range as the GIRAFFE spectra for one or two bright, early-type stars in the field. These spectra were used to calibrate the telluric absorption in the GIRAFFE spectra. Fibres not allocated to bright stars were used to obtain simultaneous spectra of the night sky.

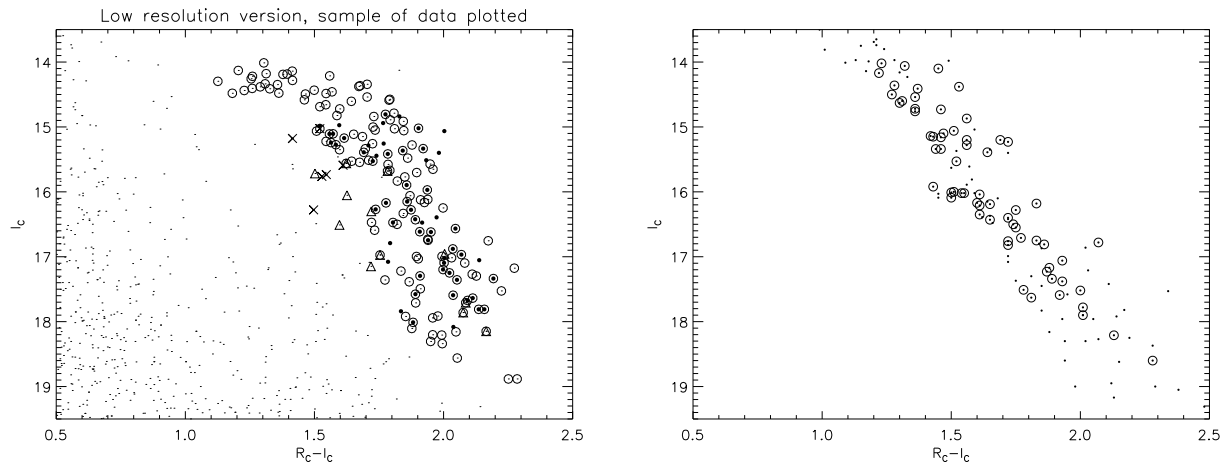


Figure 1. Colour–magnitude diagrams for stars around σ Ori (left panel) and λ Ori (right panel) with the stars we have observed highlighted (open circles). Other symbols in the left panel indicate the membership status for stars from Kenyon et al. (2005) as follows: filled circles – member; triangles – uncertain membership; crosses – non-member. This membership status was ignored during the fibre allocation process. Barrado y Navascués et al. (2004) only provide data for stars they consider to be candidate members of the λ Ori cluster so we are not able to show that position of other stars in the right panel.

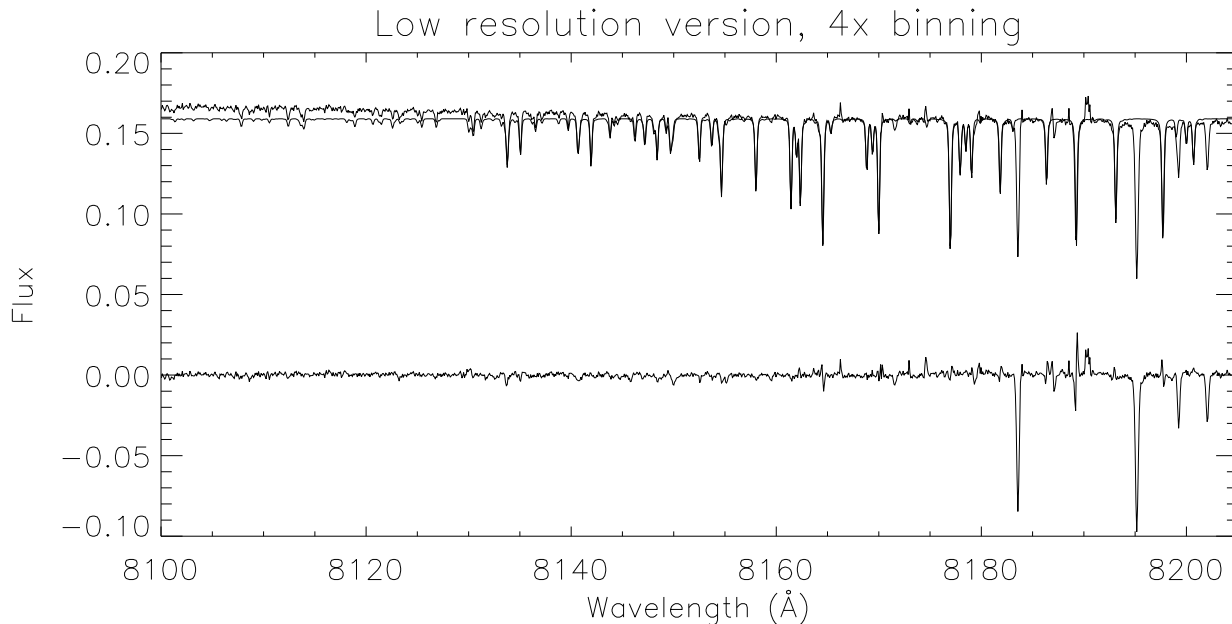


Figure 2. Example of a synthetic telluric absorption spectrum from a model terrestrial atmosphere fit to the telluric absorption in a section of one of our UVES spectra. The residuals from the fit of the synthetic absorption spectrum plus a low order polynomial are shown below the UVES spectrum and the synthetic absorption spectrum. Note that the residuals include absorption lines from the star, e.g., the Na I 8200Å doublet.

2.2 Reduction of the spectra

There is strong fringing in the images produced by the GIRAFFE spectrograph when operated at the wavelengths we have used for our observations. This makes the extraction of the spectra problematic. For brighter stars it is possible to use the spectra and their associated errors extracted from the data automatically by the ESO pipeline provided by the observatory. These spectra are extracted from the images by summing the pixels in each row within a given range around the central position of each fibre. The disadvantages of us-

ing these spectra are that there is no cosmic-ray rejection included in the extraction process and that the signal-to-noise ratio drops rapidly as the spectra become fainter.

For fainter stars we tried using the GIRAFFE Base-Line Data Reduction Software (girBLDRS) version 1.13.1 (Blecha et al. 2000) to perform optimal extraction of the spectra. This maximizes the signal-to-noise in the resulting spectra by weighting the pixels according to the variance of each pixel and a model of the spatial profile (Horne 1986). Some sort of weighted extraction is essential to pro-

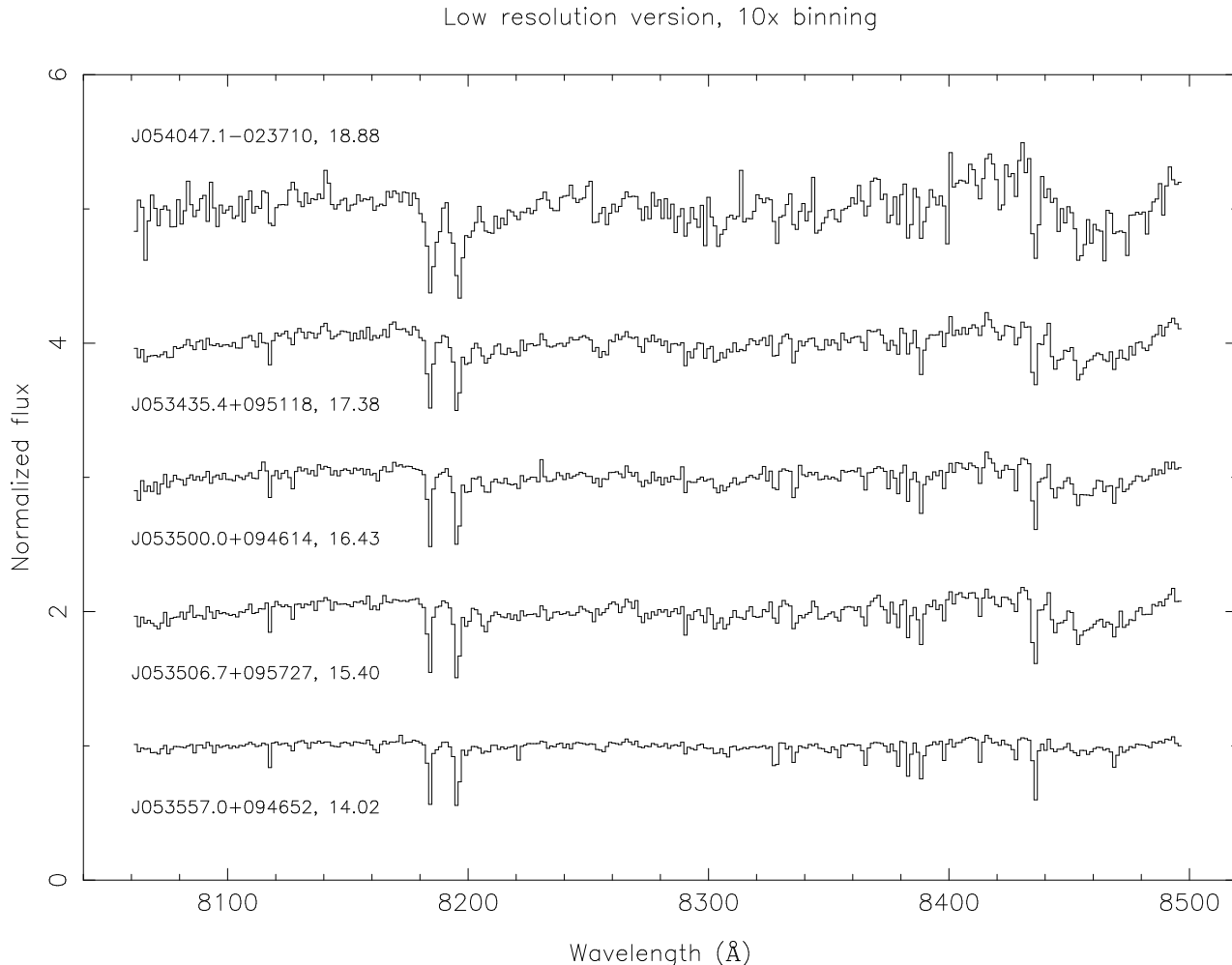


Figure 3. Example spectra of apparently single stars from our sample. The spectra of each star have been normalized by a low-order polynomial and offset for clarity and are labeled by name and I-band magnitude.

duce usable spectra for the faintest stars in our dataset. It is also possible to identify pixels affected by cosmic-rays in the images and exclude them from the extracted spectra by comparing the spatial profile of the spectra with a model. Unfortunately, we were not able to achieve the same level of stability in the radial velocities for data extracted with girBLDRS as the normal pipeline extraction. We believe that this is due to girBLDRS separately optimizing the profile used to extract the object spectra, the flat-field spectra and the thorium-argon arc spectra. The result is that the profiles used to extract the object, arc and flat spectra are slightly different. This optimization is used to account for small shifts in the positions of the spectra on the detector. The fringe-pattern can change the effective detector efficiency by about 20 percent over a spatial scale of only a few pixels and it does not move relative to the detector. Thus, using different profiles for the object, arc and flat spectra results in inaccurate flat-fielding and the introduction of spurious high-frequency noise into the spectra. This appears to be enough to reduce the precision of the radial velocities that can be measured from these spectra to $2-3 \text{ km s}^{-1}$.

For these reasons we decided to develop our own method for extracting the spectra. The key feature of the method is to use the flat-field images to create an empirical model

of the spatial profile for the spectra. This spatial profile can then be used to perform a weighted extraction of the spectra and to identify pixels affected by cosmic-rays in the images. The same weights can be used for the object frames, flat-field frames and arc frames, so the flat-fielding process does not introduce high-frequency noise into the spectra, as is the case for optimal extraction with girBLDRS. One disadvantage of this method is that small shifts in position between the flat-field images and the object frames mean that the weights applied in the extraction are not quite optimal. This results in a small reduction in the signal-to-noise ratio of the extracted spectra. A more important effect is that the flux at each wavelength is slightly underestimated and that this flux-deficit varies with wavelength and between spectra. For our GIRAFFE spectra we find that the flux-deficit is a few percent and that it varies smoothly wavelength. This only becomes a problem during the sky-subtraction phase of the data reduction. The first step in sky subtraction is to form an average sky spectrum from those fibres that were pointing at blank areas of the sky during the exposure. It is normally possible to simply subtract this average sky spectrum from the spectra of targets obtained in the same pointing. In our case, we first had to calculate an optimum scaling factor for each spectrum to be applied to the average sky spectrum

prior to subtraction. This was done by finding the scaling factor that minimized the root-mean square (RMS) difference between the sky-subtracted spectrum and a smoothed version of this spectrum.

We calculated our own dispersion solution for the spectra from the ThAr spectra obtained on the same day as the actual observations. Typical shifts over a 12 hour timescale for the GIRAFFE spectrograph are less than 0.2 pixels (Pasquini et al. 2004). We used a 6-th order polynomial fit to the positions of 22 unsaturated arc lines in the arc spectra. The worst RMS residual was 0.092\AA , the median RMS residual was 0.0045\AA . The mean dispersion of the spectra is approximately $4.9\text{ km s}^{-1}\text{ pixel}^{-1}$.

In order to correct the spectra for telluric absorption we used synthetic absorption spectra from a 6-layer model of the Earth’s atmosphere (Nicholls 1988) and the HITRAN molecular database (Rothman et al. 2005). The parameters of the model were optimized by fitting a UVES spectrum obtained at the same time as the GIRAFFE observations. The optimum fit was achieved by minimizing the mean absolute deviation from a low-order polynomial fit to the UVES spectrum after dividing through by the model spectrum. The fit to the telluric absorption was very good (Fig. 2). This synthetic telluric spectrum was convolved with a Gaussian profile to match the resolution of the GIRAFFE spectra. The synthetic telluric spectrum was then divided into the target spectra. This removed all visible traces of telluric contamination. All GIRAFFE spectra were interpolated onto a uniform velocity scale of $4.93\text{ km s}^{-1}\text{ pixel}^{-1}$ using 3200 pixels covering the wavelength range $8061.1\text{--}8496.6\text{\AA}$. We excluded spectra with a mean signal-to-noise ratio less than 5 from our analysis and also excluded stars with fewer than two such spectra. Examples of the resulting spectra for several targets are shown in Fig. 3.

3 ANALYSIS

Stars are identified in this paper by the J2000 coordinates as listed in Kenyon et al. (2005) or Barrado y Navascués et al. (2003) truncated to one decimal place in right ascension and truncated to the nearest arcsecond in declination.

3.1 Radial velocity measurements

Radial velocities for all targets were measured using cross-correlation against a template spectrum of the brown dwarf star UScoCTIO 055. This star is a visual binary with two similar components separated by only 0.12 arcsec and a combined spectral type of M5.5 (Kraus et al. 2005). We obtained 5 UVES spectra of this star from the ESO archive and formed the median average spectrum. We re-binned this spectrum onto the same wavelength scale as the GIRAFFE spectra and convolved this spectrum with a Gaussian with full-width at half-maximum (FWHM) of 3 pixels to match approximately the resolution of these spectra. Regions of the spectra affected by strong sky line emission were excluded from the cross-correlation. The radial velocity (RV) derived from the position of the peak of cross-correlation function (CCF) and its error was measured using a parabolic fit to the three points at the top of the CCF. The RV of UScoCTIO 055 was taken to be -6.38 km s^{-1} (Kurosawa et al. 2006).

Table 2. Radial velocities, V_r , of stars in σ Ori and λ Ori. The date of observation is given as modified heliocentric Julian date (MHJD). The standard error of the RV given here includes the “external error” and zero-point correction measured from the sky lines described in the text. The full-width at half-maximum of the cross-correlation function is given in the final column. *The full version of this table is only available in the on-line version of this paper.*

Star	MHJD	V_r (km s^{-1})	FWHM (km s^{-1})
J053557.0+094652	53657.309	28.89 ± 0.67	63
J053557.0+094652	53691.200	28.52 ± 0.60	63
J053557.0+094652	53734.145	28.74 ± 0.68	63
J053539.4+095032	53657.309	27.22 ± 0.68	69
J053539.4+095032	53691.200	27.31 ± 0.61	70
J053539.4+095032	53734.145	27.82 ± 0.69	68
J053530.4+095034	53657.309	28.70 ± 0.71	116
J053530.4+095034	53691.200	28.09 ± 0.66	116
J053530.4+095034	53734.145	28.77 ± 0.72	113

The precision with which the peak of the CCF can be measured is unlikely to be a true reflection of the accuracy with which we can measure the radial velocities from our spectra. In order to quantify the accuracy of our radial velocities we measured the radial velocities of the night sky emission lines in our spectra. We used the night sky emission line spectrum observed with the UVES spectrograph as a template in the cross-correlation (Hanuschik 2003). We measured all the spectra observed at a given pointing, including object spectra prior to sky-subtraction, and calculated the mean and standard deviation of the resulting radial velocities. The standard deviation, σ_{sky} , is given in Table 1. The mean RV shift of the sky-line spectra for a given pointing ranges from -1.28 km s^{-1} to -0.25 km s^{-1} . We have subtracted this mean radial velocity shift from the measured radial velocities of our targets, i.e., the night sky emission line spectrum is used to define the zero-point of the stellar radial velocities at each pointing. We have also added the value of σ_{sky} for each frame in quadrature to the precision of the stellar RV measured from the cross correlation function. For 85 percent of our RV measurements σ_{sky} is the dominant term in the uncertainty. The resulting RV measurements with their standard deviations are given in Table 2.

3.2 Variability criterion for radial velocities

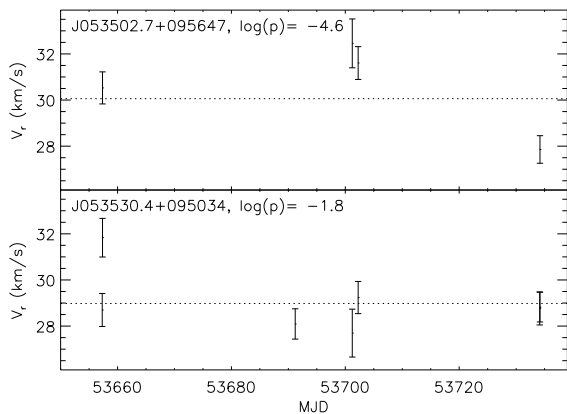
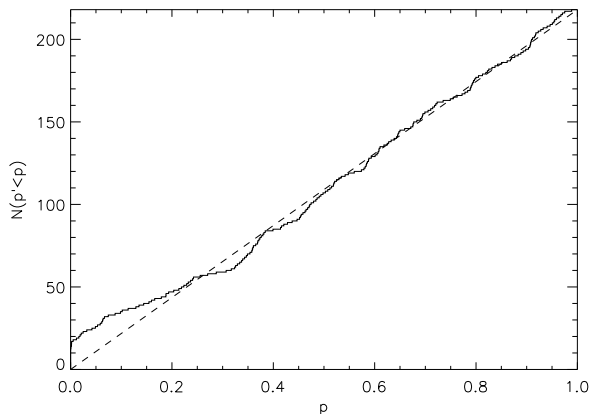
For each star we have N_{rv} RV measurements $V_{r,i}$ each with standard error σ_i . We calculate the weighted mean RV for each star, \bar{V}_r , and then calculate the chi-squared statistic for \bar{V}_r as a model for the observed radial velocities, i.e.,

$$\chi^2 = \sum_{i=1}^{N_{\text{rv}}} \frac{(V_{r,i} - \bar{V}_r)^2}{\sigma_i^2}$$

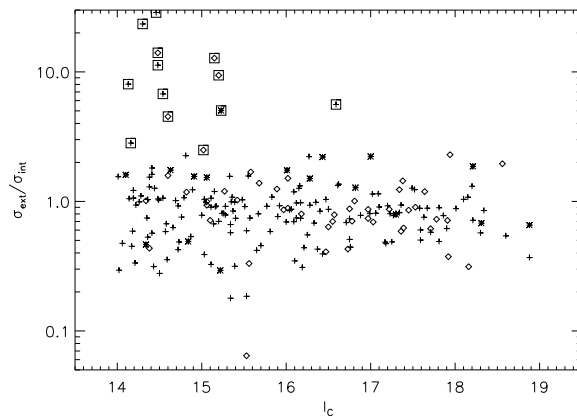
In order to identify stars with variable radial velocities we calculate the probability p of observing this value of χ^2 or greater from a sample of normally distributed random observations with mean \bar{V}_r and standard errors σ_i . Our criterion for identifying stars with variable radial velocities is $\log(p) < -4$. The probability that one or more stars

Table 3. Summary of measurements for each target. *The full version of this table is only available in the on-line version of this paper.*

Star	I_C (mag)	N_{rv}	\bar{V}_r (km s^{-1})	$\log(p)$	EW(Na I) (\AA)	TiO(8442)
J053557.0+094652	14.02	3	28.70 ± 0.37	-0.04	2.34 ± 0.01	0.677 ± 0.001
J053539.4+095032	14.06	3	27.44 ± 0.38	-0.10	2.34 ± 0.02	0.667 ± 0.002
J053530.4+095034	14.10	7	28.98 ± 0.44	-1.76	2.33 ± 0.01	0.668 ± 0.001
J053502.7+095647	14.16	4	30.06 ± 1.01	-4.57	2.33 ± 0.02	0.663 ± 0.001
J053408.4+095125	14.17	4	6.52 ± 0.34	-0.05	2.61 ± 0.02	0.637 ± 0.001
J053426.0+095149	14.36	4	-0.65 ± 0.34	-0.08	2.85 ± 0.01	0.657 ± 0.001
J053555.6+095053	14.38	3	27.26 ± 0.39	-0.08	2.53 ± 0.02	0.682 ± 0.002

**Figure 4.** Example radial velocity measurements as a function of time. The star identifier and value of $\log(p)$ are indicated in each panel. The weighted mean radial velocity is indicated by a dotted line.**Figure 5.** Left panel: Cumulative distribution of p . The difference between this distribution and a uniform distribution (dashed line) is not significant.

are incorrectly identified as having variable radial velocities by chance due to statistical fluctuations (assumed to be normally distributed) in our sample of 218 stars is about 2 percent. The values of N_{rv} , $\log(p)$ and \bar{V}_r for each target are given in Table 3. There are two ways to calculate

**Figure 6.** The ratio of the standard errors of the mean radial velocities, σ_{ext} and σ_{int} , as a function of I_C magnitude. The width of the CCFs is indicated as follows: crosses, $\text{FWHM} < 80 \text{ km s}^{-1}$; diamonds, $80 \text{ km s}^{-1} < \text{FWHM} < 100 \text{ km s}^{-1}$; asterisks, $\text{FWHM} > 100 \text{ km s}^{-1}$. Stars with significantly variable radial velocities are highlighted (squares).

the standard error of the weighted mean, the external error based on the scatter of the data,

$$\sigma_{\text{ext}} = \sqrt{\frac{\chi^2}{(N_{rv} - 1) \sum 1/\sigma_i^2}},$$

and the internal error based on the standard errors only,

$$\sigma_{\text{int}} = \sqrt{\frac{1}{\sum 1/\sigma_i^2}}.$$

The value given in Table 3 is the larger of these two values.

There are 12 stars in our sample that have variable radial velocities according to our criterion $\log(p) < -4$. The properties of these stars are listed in Table 4. Stars in which both components are visible in the spectra or CCFs are identified as SB2, those showing only a single spectrum are identified as SB1. Examples of radial velocities for stars with $\log(p) < -4$ and $\log(p) > -4$ are shown in Fig. 4.

If our values of σ_i are good estimates of the true uncertainty on each RV measurement and the majority of stars in our sample are non-variable, then we would expect that the distribution of p will be uniform. The cumulative distribution of our measured p values is compared to a uniform distribution in Fig. 5. We have tested the hypothesis that these two distributions are equal using the Kolmogorov-Smirnov

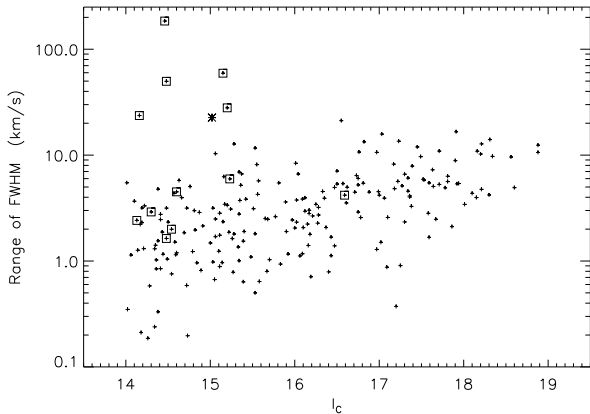


Figure 7. The range in full-width at half maximum (FWHM) of the cross-correlation function (CCF) for each target as a function of I_C magnitude. Stars with variable radial velocities are highlighted (squares). The SB2 binary J054001.0–021959 discussed in the text is marked with an asterisk.

test and find that there is no evidence for any significant difference between them.

We have also tested the reliability of our σ_i values by considering the ratio $Z = \sigma_{\text{ext}}/\sigma_{\text{int}}$. If the values of σ_i are reliable then we expect $Z \approx 1$. More precisely, for samples drawn from normal distributions the mean value of Z is 1 with standard error $1/\sqrt{2(N_{\text{rv}} - 1)}$ (Topping 1962). The values of Z for our RV measurements are shown as a function of I_C magnitude in Fig. 6. It can be seen that the values of Z are indeed close to 1 (with the exception of the spectroscopic binaries, of course) and that there is no significant trend of Z with I_C . Stars with broad spectral lines are highlighted in this figure so that it can also be seen that the values of Z are not significantly different for rapidly rotating stars compared to other stars in the sample.

3.3 Binary stars identified from variable line width

In Fig. 7 we show the range in the FWHM of the CCFs against I_C magnitude. We have used this plot to identify potential SB2 binary stars in which blending of the spectra from two similar components results in variations in the width of the spectral lines with little change in the radial velocity measured from the peak of the CCF. Several of the SB2 binaries identified above are recovered by this method. The star J054001.0–021959 has a large range in FWHM compared to other stars of the same I_C magnitude. The four spectra of this star all have high signal-to-noise. There is a definite broadening and asymmetry in one spectrum (Fig. 8). In addition, the value of $\log(p)$ for this star is close to our criterion for variable radial velocities. This star appears to be an SB2 binary. One other star (J053522.5+094501) has a range in FWHM $> 20 \text{ km s}^{-1}$, but this is a result of two spectra of the seven obtained having low signal-to-noise. There is no sign of asymmetry in the CCF and the radial velocities of this star show no hint of variation ($\log(p) = -0.09$). Despite the large range of FWHM measured for this star, there is no strong evidence that it is an SB2 binary star.

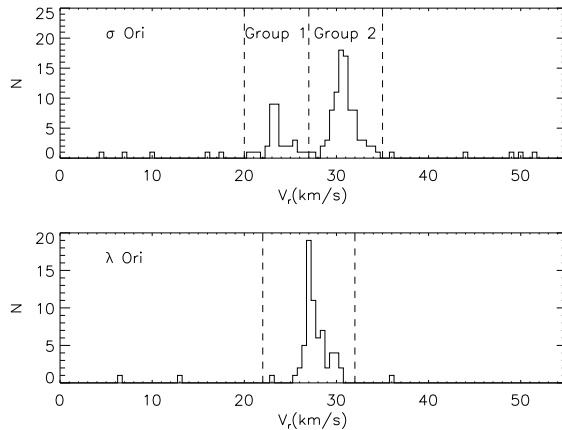


Figure 9. The distributions of weighted mean radial velocity for our targets in λ Ori and σ Ori. Dashed lines show the selection criteria for assigning stars to Group 1 or Group 2 for σ Ori and for selecting non-members for both clusters, as described in section 3.4.

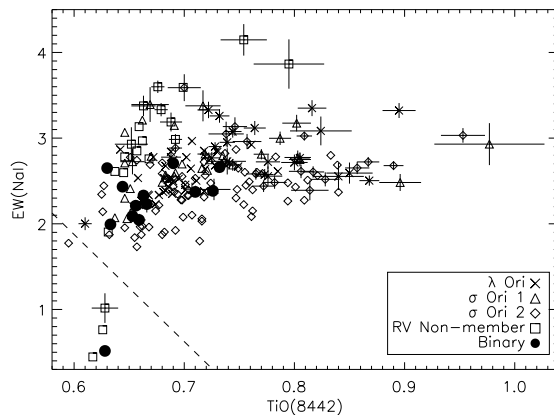


Figure 10. The value of $\text{EW}(\text{NaI})$ versus the $\text{TiO}(8442)$ spectral index for our targets. The plotting symbols used indicate binarity or membership of the σ Ori or λ Ori clusters or non-membership of these clusters based on the radial velocity (if non-variable), as indicated in the legend. Stars below the dashed line are considered to be non-members. Error bars are only shown in cases where they are larger than the plotting symbol used.

3.4 Membership criteria

In this section we describe the criteria we have used to identify members of the σ Ori and λ Ori associations. The principal means of identifying members of these clusters is the mean RV of the star, but we have also used the equivalent width of the NaI doublet, $\text{EW}(\text{NaI})$, and the strength of the TiO band at 8442\AA , $\text{TiO}(8442)$, as additional membership criteria.

The distributions of weighted mean radial velocities, \bar{V}_r , are shown separately for stars near σ Ori and λ Ori in Fig. 9. The bi-modal distribution of radial velocities for stars near σ Ori discussed by Jeffries et al. (2006) is apparent. We follow the convention in that paper of assigning stars with $\bar{V}_r < 27 \text{ km s}^{-1}$ to Group 1 and stars with $\bar{V}_r \geq 27 \text{ km s}^{-1}$ to Group 2. The interpretation of these groups favoured

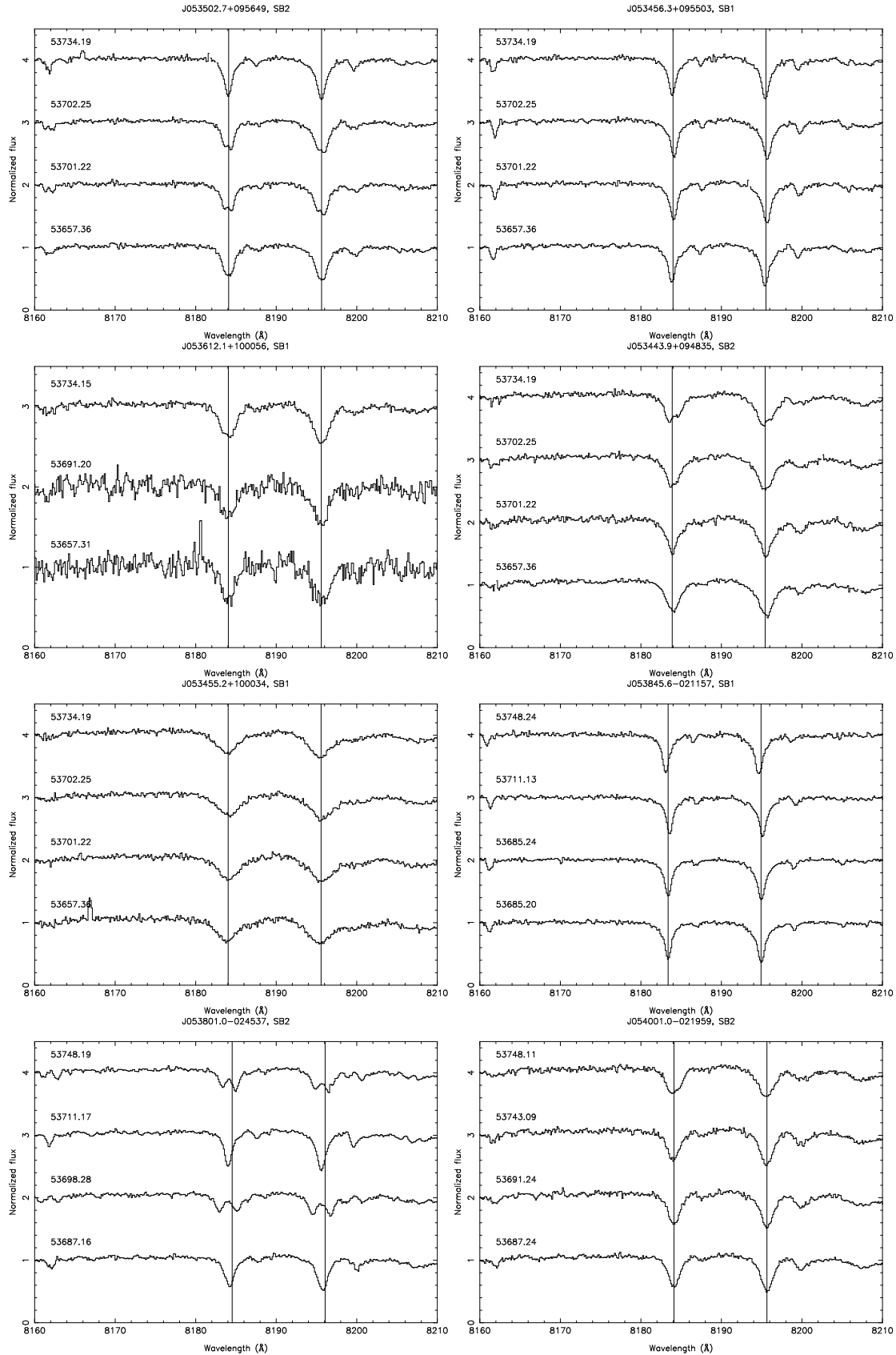


Figure 8. Spectra of the spectroscopic binaries discovered by our survey around the Na I 8200 feature. The spectra have been normalized using a low-order polynomial and offset for clarity. Spectra are labeled by the modified heliocentric JD of observation. The wavelengths of the Na I doublet at the mean radial velocity of the star are marked by vertical lines.

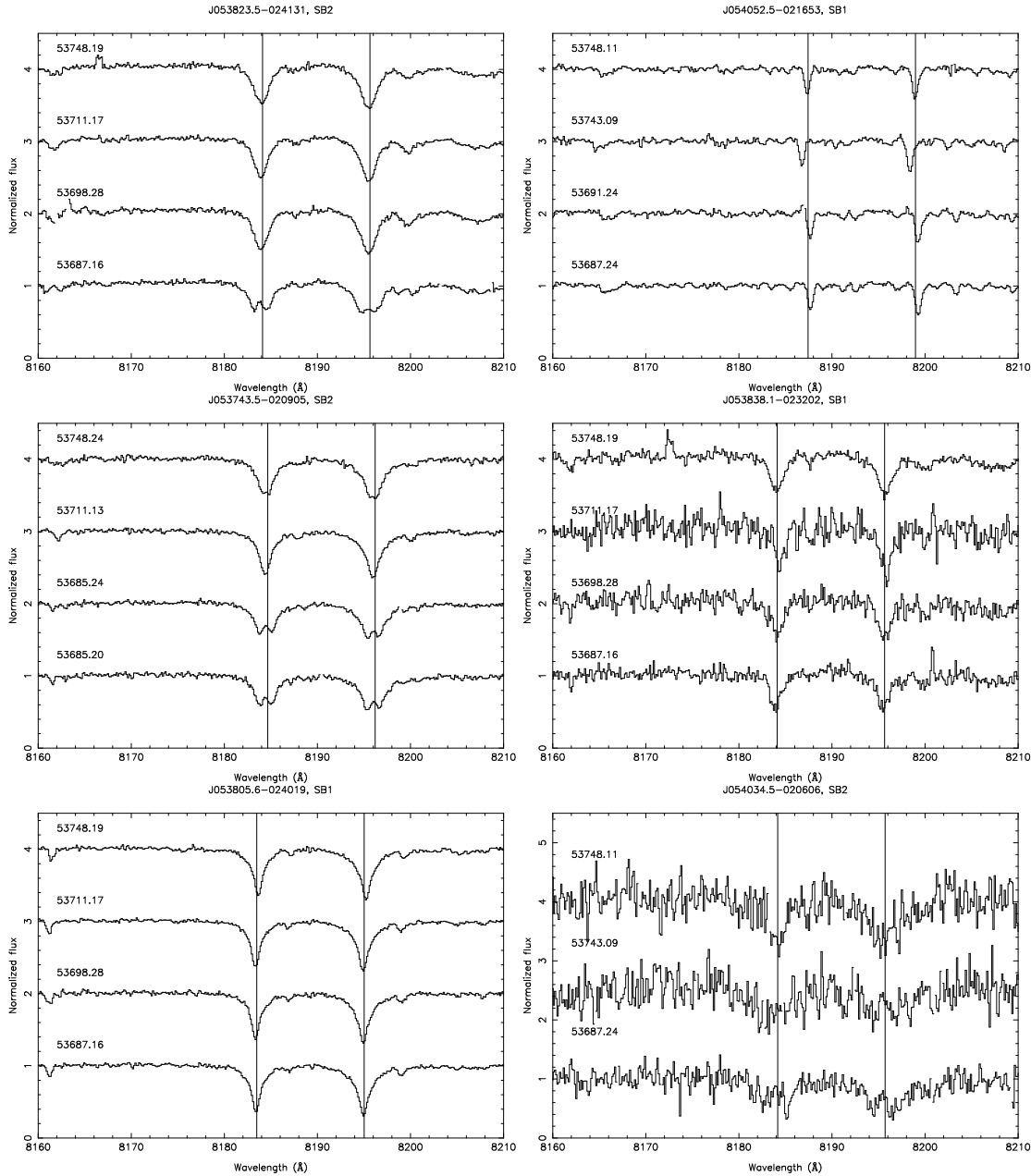


Figure 8 – continued

by Jeffries et al. is that Group 1 are members of either the Orion OB1a or OB1b association while Group 2 are a separate cluster of stars associated with the star σ Ori. Group 2 are concentrated spatially around the star σ Ori and have similar mean radial velocity to it. Group 2 are younger on average than Group 1, although considerable overlap is possible.

For stars near σ Ori we identify non-members using the criterion $\bar{V}_r > 35\text{km s}^{-1}$ or $\bar{V}_r < 20\text{km s}^{-1}$. For stars near λ Ori we identify non-members using the criterion $\bar{V}_r > 32\text{km s}^{-1}$ or $\bar{V}_r < 22\text{km s}^{-1}$. These limits are indicated in Fig. 9. The application of these criteria to stars with variable radial velocities are discussed in more detail in section 4.

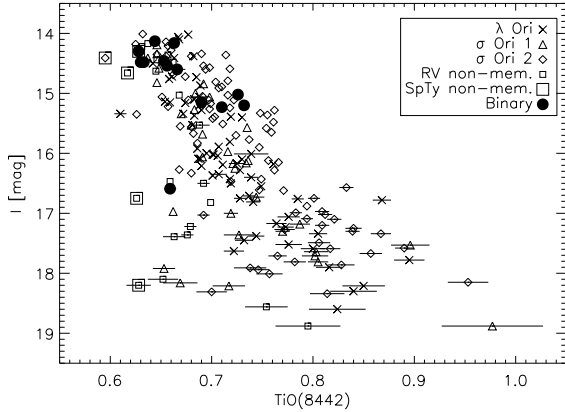
The TiO bands around 8450\AA are good indicators of effective temperature for M-dwarfs in the sense that they in-

crease in strength for cooler stars (Mohanty et al. 2004) and are insensitive to reddening. We have measured the strength of the band at 8442\AA in our spectra using the ratio of the counts detected in the wavelength ranges $8437-8442\text{\AA}$ and $8442-8450\text{\AA}$. The measurements were made on the median average spectrum of each star. We denote the value of this ratio as TiO(8442).

The equivalent width of the NaI doublet at 8190\AA is sensitive to the surface gravity in M-type stars (Schiaon et al. 1997) in that stars with higher surface gravities show stronger NaI absorption. The surface gravity of members of the σ Ori and λ Ori clusters is expected to be $\log g = 3-4$, whereas a typical M-type giant will have $\log g \approx 1$. Thus, the equivalent width of the NaI doublet, EW(NaI), can be used to identify background giants in our

Table 4. Properties of the binaries discovered by our survey. The standard error in the mean for the measured radial velocities is listed under σ_{rv} . Non-members of the clusters are indicated in the final column by the note ‘nm’.

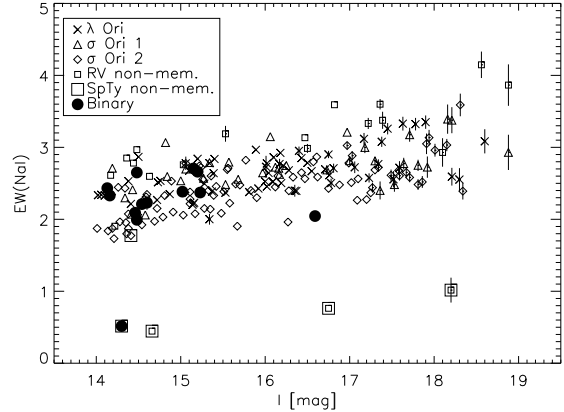
Star	I_C (mag)	$R_C - I_C$ (mag)	N_{rv}	\bar{V}_r (km s^{-1})	σ_{rv} (km s^{-1})	$\log(p)$	EW(NaI) (\AA)	TiO(8442)	Notes
J053502.7+095649	14.16	1.30	4	30.06	1.01	-4.6	2.33 ± 0.02	0.663 ± 0.001	SB2
J053456.3+095503	14.54	1.36	4	26.20	2.32	-28.8	2.21 ± 0.01	0.656 ± 0.001	SB1
J053612.1+100056	14.60	1.31	3	28.66	2.68	-8.9	2.23 ± 0.10	0.666 ± 0.008	SB1
J053443.9+094835	15.20	1.69	4	22.56	3.48	< -42	2.66 ± 0.02	0.732 ± 0.002	SB2
J053455.2+100034	15.23	1.72	4	27.92	2.20	-15.6	2.37 ± 0.02	0.710 ± 0.002	SB1 ^a
J053845.6-021157	14.48	1.18	4	4.11	3.52	< -42	1.99 ± 0.02	0.633 ± 0.001	SB1
J053801.0-024537	14.46	1.57	4	46.12	9.20	< -42	2.09 ± 0.01	0.653 ± 0.001	SB2
J054001.0-021959	15.02	1.90	4	30.80	0.90	-3.5	2.38 ± 0.02	0.726 ± 0.003	SB2 ^b
J053823.5-024131	15.15	1.69	4	30.23	4.26	< -42	2.71 ± 0.02	0.690 ± 0.002	SB2
J054052.5-021653	14.30	1.13	4	152.28	8.25	< -42	0.52 ± 0.02	0.628 ± 0.001	SB1, nm
J053743.5-020905	14.48	1.36	4	51.02	4.76	< -42	2.65 ± 0.02	0.630 ± 0.001	SB2
J053838.1-023202	16.59	1.73	4	30.79	2.65	-19.5	2.05 ± 0.07	0.659 ± 0.006	SB1
J053805.6-024019	14.13	1.21	4	7.68	2.53	-41.1	2.43 ± 0.01	0.644 ± 0.001	SB1

^a Hint of companion in CCF.^b Identified from variation in width of CCF.**Figure 11.** The TiO(8442) spectral index versus I-band magnitude for our targets. The plotting symbols used indicate binarity or membership of the σ Ori or λ Ori clusters or non-membership of these clusters based on the radial velocity or spectral type (see Fig. 10), as indicated in the legend. Error bars are only shown in cases where they are larger than the plotting symbol used.

sample. It is also possible to identify contamination of the sample by dwarf stars with $\log g \gtrsim 4.5$. We measured the value of EW(NaI) from the median average spectrum of each star by numerically integrating the area under our spectra in two regions $\pm 120 \text{ km s}^{-1}$ wide around the centre of each NaI line after normalizing the spectra by the clipped mean value of the spectrum in the region 8188–8192 \AA .

The value of TiO(8442) is plotted against EW(NaI) in Fig. 10. There is a clear division between the bulk of our targets and the small group of stars with low EW(NaI) and TiO(8442) values. Most of these stars are non-members based on their mean RV. We therefore identify all stars below the dashed line in this figure as ‘spectral-type non-members’.

From Figs. 11 and 12 we see that very few stars that

**Figure 12.** The equivalent width of the NaI doublet for our targets as a function of the I-band magnitude. The plotting symbols used indicate binarity or membership of the σ Ori or λ Ori clusters or non-membership of these clusters based on the radial velocity or spectral type (see Fig. 10), as indicated in the legend. Error bars are only shown in cases where they are larger than the plotting symbol used.

satisfy the RV and spectral type criteria for membership have discrepant values of EW(NaI) or TiO(8442) for their I_C magnitude. There are two faint stars in the sample that have large values of TiO(8442), but there is a large scatter in this index among the faint stars in our sample so we do not consider this to be a reason to exclude these stars as members of the σ Ori cluster.

The binary star with a discrepant value of EW(NaI) is J054052.5-021653. This SB1 binary star has weak, narrow NaI absorption lines characteristic of a giant star. The mean RV has a rather large uncertainty but is also clearly inconsistent with membership of the σ Ori cluster. We conclude that this is a background giant star.

The spectra of the star J054034.5-020606 extracted us-

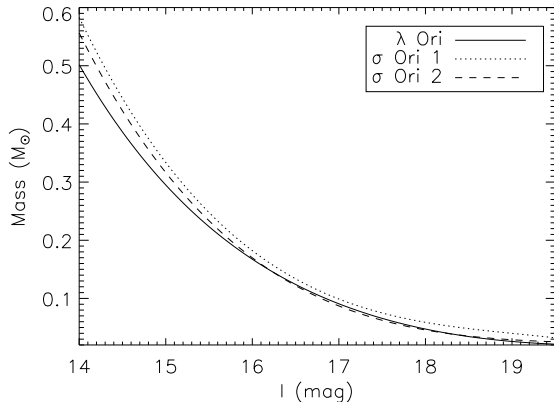


Figure 13. The I-band mass-magnitude relations interpolated from the models of Baraffe et al. (1998) for the following distances and ages: $d=330\text{pc}$, $\text{age}=10\text{ Myr}$ (σ Ori 1); $d=440\text{ pc}$, $\text{age}=3\text{ Myr}$ (σ Ori 2); $d=400\text{ pc}$, $\text{age}=5\text{ Myr}$ (λ Ori).

ing our empirical weighting scheme do not satisfy our criterion for inclusion in the sample because the signal-to-noise is less than 5 but we did notice that this is an SB2 spectroscopic binary from an analysis of the spectra extracted using girBLDRS. These spectra are shown in Fig. 8. This is the faintest binary detected in our survey ($I_C = 18.38$) so the spectra are quite noisy, but the SB2 nature of this star can be seen and is very obvious in the CCF. The values $\text{EW}(\text{NaI}) = 3.42 \pm 0.23$ of $\text{TiO}(8442) = 0.593 \pm 0.026$ shows that this star has the wrong spectral type to be a member of the σ Ori cluster. We have also inspected the position of this star in the V v. $V-I_C$ colour-magnitude diagram of the σ Ori region using the data of Mayne et al. (2007), where it is clearly below the sequence of cluster members. We conclude that this is a background dwarf binary star for which the combination of spectral type, distance and reddening place the star within the band of cluster members in the I_C v. $R_C - I_C$ colour-magnitude diagram.

Having applied these membership selection criteria we find that in our sample there are 64 members of λ Ori, 34 members of σ Ori Group 1 and 86 members of σ Ori Group 2, excluding stars with variable radial velocities that are discussed separately below.

4 BINARY STARS IN OUR SAMPLE

In this section we discuss the stars in our sample with variable radial velocities or variable line profiles that are members of the σ Ori or λ Ori clusters. The values of \bar{V}_r , $\text{TiO}(8442)$, etc. for these stars are given in Table 4. The spectra of these stars in the region of the NaI doublet are shown in Fig. 8.

We also note in Table 4 whether only one set of spectral lines are visible (SB1) or that the spectra indicate the presence of two stars (SB2). A star may be an SB1 binary either because the companion is too faint to be detectable or because the lines of the stars are blended, or both. We created a set of synthetic binary star spectra using combinations of observed single star spectra over a range of luminosity ratio and radial velocity difference to estimate the lower limit

to the magnitude difference in the SB1 stars. If we assume that neither star is rapidly rotating then we estimate that any companion to these stars is more than 2.5 magnitudes fainter than the primary. From the magnitude-mass relation shown in Fig. 13 we estimate that the corresponding limit to the mass ratio is $q \lesssim 0.25$.

In general, the $I_C R_C$ photometry, the values of $\text{TiO}(8442)$, $\text{EW}(\text{NaI})$ and the mean RV of these stars are all consistent with membership of either the λ Ori cluster or one of the σ Ori clusters. We discuss exceptions to this general rule and any other points of interest for these stars below.

J053502.7+095649 Barrado y Navascués et al. (2004) consider this star (LOri-CFHT 043) to be a member of the λ Ori cluster on the basis of the available $R_C I_C$ JHK photometry.

J053443.9+094835 Barrado y Navascués et al. (2004) note that the position of this star (LOri-CFHT 069) in the I_C v. $I_C - K_S$ colour-magnitude diagram is inconsistent with cluster membership. However, this is simply a result of the contribution of two stars of similar brightness to the flux at I-band in this SB2 binary (Fig. 8). Correcting the I-band magnitude by 0.75 magnitudes places this star in a position entirely consistent with cluster membership in this colour-magnitude diagram.

J053455.2+100035 Barrado y Navascués et al. (2004) note the presence of $H\alpha$ emission in their low resolution spectrum of this star (LOri-CFHT 075). The position of this star in the $I_C - K_S$ v. $H - K_S$ colour-colour diagram and the I_C v. $I_C - K_S$ colour-magnitude diagram are also consistent with cluster membership and with the spectral type of M5 assigned by Barrado y Navascués et al. (2004) so it is unclear why they note it as being a non-member on the basis of this information in their Table 2. The spectral lines for this star show rotational broadening. We compared the spectra of this star to those of a narrow-lined star of similar spectral type to which we had applied a rotational broadening function for various values of the projected rotational velocity, $V_{\text{rot}} \sin i$. From this comparison we estimate that the projected rotational velocity of J053455.2+100035 is $V_{\text{rot}} \sin i \approx 65\text{ km s}^{-1}$. Only one set of spectral lines are visible in our spectra but there is an asymmetry in the CCF in the form of a blue-wing, particularly when the measured RV corresponds to a red-shift. This suggests that the fainter component in this binary is detected but unresolved in the I-band spectra.

J053845.6-021157 The range in radial velocities we have observed for this star is -6.9 to 11.2 km s^{-1} . This is consistent with this star being a member of σ Ori Group 1 if it has a semi-amplitude $\approx 30\text{ km s}^{-1}$. Members of Group 1 are approximately twice as common as members of Group 2 in the 25 arcmin GIRAFFE field used for the observations of this star. The orbital period is required to be rather short ($P \lesssim 1\text{ day}$) to reconcile the observed radial velocities of this star with a mean velocity consistent with cluster membership and the expected mass ratio for an SB1 binary ($q \lesssim 0.25$).

J053801.0-024537 The mean RV estimated from the spectra is consistent with membership of either σ Ori Group 1 or σ Ori Group 2. There are approximately 10 times as many members of Group 2 as Group 1 in this field close to

σ Ori so we conclude that it is approximately 10 times more likely that this star is a member of Group 2 than Group 1. The values of EW(NaI) and TiO(8442) for this star were measured from the spectrum observed near conjunction.

J054001.0–021959 Kenyon et al. (2005) detected strong lithium absorption in the spectrum of this star (KJN2005 6), which indicates that this star is younger than 20Myr, as expected for a member of the σ Ori cluster. The mean RV of this star suggests it is more likely to be a member of σ Ori Group 2 than Group 1.

J053823.5–024131 The mean RV measured from the three spectra in which the two components are unresolved is $26.5 \pm 0.9 \text{ km s}^{-1}$, which is close to the dividing line at 27 km s^{-1} between Group 1 and Group 2. The proximity of this star to σ Ori makes it approximately 10 times more likely that this is a member of Group 2 than Group 1. This star (BMZ2001 S Ori J053823.6–024132) was listed as a candidate member of the σ Ori cluster on the basis of IJHK photometry by Béjar et al. (2004).

J053743.5–020905 We measured the value of EW(NaI) and TiO(8442) for this SB2 binary from the spectrum taken near conjunction, so the values represent an average value for the two stars, which are of comparable brightness. The RV measured from this spectrum is 42 km s^{-1} , which is outside the range we have defined for membership of the σ Ori cluster, but it is difficult to establish whether this is an accurate estimate of the mean RV of this star. Further observations will be required to establish the true mean RV of this binary star in order to check that it is consistent with this star being a cluster member. Members of Group 1 are approximately twice as common in this field as Group 2 (Jeffries et al. 2006). For the purposes of this paper we assume that this star is a cluster member.

J053838.1–023202 The mean RV of this SB1 binary and its proximity to σ Ori suggest that it is a member of Group 2.

J053805.6–024019 The range of radial velocities observed in this SB1 binary star is 4.4 to 14.5 km s^{-1} , which is consistent with membership of σ Ori if the semi-amplitude of the spectroscopic orbit is $K \approx 20 \text{ km s}^{-1}$. The proximity of this star to σ Ori makes it approximately 10 times more likely that this is a member of Group 2 than Group 1.

In summary, we have identified 5 spectroscopic binary members of the λ Ori cluster and 7 spectroscopic binary members of the σ Ori cluster. Among the σ Ori spectroscopic binaries, 5 stars are likely to be members of Group 2, 1 is likely to be a member of Group 1 and 1 star cannot be assigned to either group. Of the 12 spectroscopic binary cluster members, 6 are SB2 binaries with stars of comparable brightness in the I-band. There is 1 SB1 binary with broad lines due to rotation so it is not clear whether this is a genuine SB1 binary or an unresolved SB2 binary, although there is a hint of the companion in the CCF for this star. There are 3 SB1 binaries with narrow lines for which we can say the companion is likely to be more than 2.5 magnitudes fainter than the primary so that the mass ratio is less than about 0.25. We have also identified two spectroscopic binaries that are not members of either σ Ori or λ Ori.

4.1 The distribution of binaries with magnitude

It is notable that all 12 spectroscopic binary stars we have identified among the 196 cluster members are brighter than $I_C = 16.6$, and 11 are brighter than $I_C = 15.25$. There are 68 cluster members brighter than $I_C = 15.25$ including these binary stars. At face value, this suggests a close binary fraction of about 16 percent above this limit and less than a few percent below this limit. Of course, the sensitivity of our survey decreases for fainter stars because the signal-to-noise of the spectra is less and the orbital speeds decrease with mass for a given semi-major axis or orbital period.

We have used the RV data for the 11 binary cluster members we detected from their RV variations to estimate the sensitivity of our survey to binaries of this type as a function of I-band magnitude, $p_{\text{empirical}}$. We exclude J054001.0–021959 from this analysis because it is unclear how to simulate the method by which we detected this binary, i.e., from the variation of the width of its CCF. For every combination of variable and non-variable star in our survey we have created a synthetic RV dataset using the RV errors in the non-variable star dataset and the radial velocities of the binary star scaled as follows. We first subtract our best estimate of the systemic radial velocity for the binary. We then estimate the total mass of the binary, m_T assuming that the stars are identical for the SB2 binaries or that the companion is 2.5 magnitudes fainter than the primary for the SB1 binaries. The masses are estimated using the models of Baraffe et al. (1998) based on the I_C magnitude of the target. The relations between I_C and mass are shown in Fig. 13. We have assumed the following distances and ages for the clusters: $d=330 \text{ pc}$, $\text{age}=10 \text{ Myr}$ (σ Ori 1); $d=440 \text{ pc}$, $\text{age}=3 \text{ Myr}$ (σ Ori 2); $d=400 \text{ pc}$, $\text{age}=5 \text{ Myr}$ (λ Ori). We then repeat the calculation to find the total mass, m_T , of a similar binary star with the same I_C magnitude as the single star, m_S . We then multiply the radial velocities by $\sqrt{m_S/m_T}$. This is equivalent to assuming that the distribution of semi-major axis is independent of mass. We then apply the same detection criterion as before ($\log(p) < -4$) to the synthetic datasets. In cases where N_{rv} is less for the single star than the binary star we use the average number of detections for all combinations of N_{rv} synthetic radial velocities from the combinations available. For cases where N_{rv} is larger for the single star than the binary star we use the N_{rv} measurements with the lowest RV errors to create the synthetic dataset. The number of synthetic RV data sets which satisfy our variability criterion then gives an estimate of the detection efficiency for each star, e.g., if 6 of the 11 synthetic RV data sets for a star satisfy our variability criterion, then the same observations of a binary star similar to those discovered in this survey with the same I_C magnitude would, on average, have detected a significant RV shift about 55 percent of the time. The values of $p_{\text{empirical}}$ calculated in this way is shown in Fig. 14 as a function of the I_C magnitude.

The normalized cumulative distribution function for these detection efficiencies is shown as a function of I_C magnitude in Fig. 15. Also shown is the cumulative distribution function for the I_C magnitude of the binary cluster members excluding J054001.0–021959. If the binary fraction and semi-major axis distribution for binaries is independent of mass then these two distribution should be the

same. It is clear that the two distributions are not the same. The Kolmogorov-Smirnov test applied to these distributions gives a 99.7 percent significance level to the difference in these distributions. There is a chance that a few of the stars we have identified as SB1 binary stars are the result of spurious RV shifts due to errors in the analysis or instrumental effects or the result of intrinsic variability of a single star. If we take a very cautious approach and repeat this analysis using the detections of SB2 binaries only we find that Kolmogorov-Smirnov test gives significance level of 97.6 percent.

4.2 The binary fraction

We used a Monte-Carlo simulation to calculate probability distribution for the binary fraction given the 11 binaries we have discovered from their variable radial velocities and the detection efficiency for each star, $p_{\text{empirical}}$, calculated above.

The results are shown in Fig. 16 for the whole sample, a ‘bright’ sample ($I_C < 16.9$) and a ‘faint’ sample ($I_C \geq 16.9$). The division here between the bright and faint samples has been chosen to correspond to the widely accepted division between low mass stars and VLM stars at a mass of $0.1M_{\odot}$ (Burgasser et al. 2007). The mean value of $p_{\text{empirical}}$ for the 145 stars in the bright sample is 0.89. For the 51 stars in the faint sample the mean value of $p_{\text{empirical}}$ is 0.53. The spectroscopic binary fraction for the bright sample is $9.5^{+1.2}_{-2.8}$ percent. The 90 percent confidence upper limit to the spectroscopic binary fraction for the faint sample, given the assumptions above, is 7.5 percent. These figures apply to binary stars of the type discovered by our survey only, i.e., we have not attempted to apply a correction to this spectroscopic binary fraction for the binaries at longer orbital periods that are not detected by our survey. The hypothesis that f_{bright} and f_{faint} are equal can be rejected with 90 percent confidence. The value of $I_C = 16.9$ that is used as the dividing line between the faint and bright samples is arbitrary. It would be possible to achieve a higher level of significance by setting the limit between our bright and faint samples closer to magnitude of the faintest binary in our sample ($I_C = 16.5$), but this would be an equally arbitrary value and so it would be hard to justify the apparent increase in statistical significance.

4.3 The detection efficiency as a function of binary separation

We have used another Monte Carlo simulation to estimate the range of semi-major axis, a , over which binary stars can be detected by our survey.

If binarity is the only cause of variable RVs, the probability that a given target is flagged as an RV variable is given by $\epsilon_b p_{\text{detect}} + (1 - \epsilon_b)10^{-4}$, where ϵ_b is the overall binary fraction and p_{detect} is the probability that $\log p < -4$ for the object assuming that it is a binary.

We have used a Monte Carlo simulation to calculate the value of p_{detect} as a function of semi-major axis, a , for every star in our sample given various assumptions about the distribution of binary properties. The simulation generates 65536 virtual binaries and predicts the RV of the more massive component at the same times of observation as the

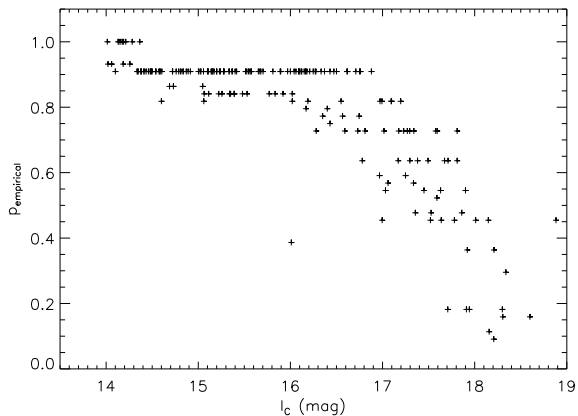


Figure 14. The detection efficiency as a function of magnitude for our survey based on the radial velocities of the binaries identified from their radial velocity variations.

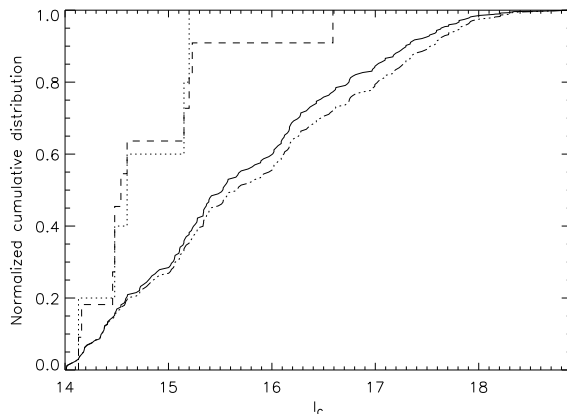


Figure 15. The normalized cumulative distribution of the detection efficiency of our sample as a function of I_C magnitude based on the measured radial velocities of all binaries detected (solid line) or the SB2 binaries only (dashed-dotted line) compared to the normalized cumulative distribution of I_C magnitude for all the binaries discovered by our survey (dashed line) and the SB2 binaries discovered by our survey (dotted line).

actual observations. The eccentricity, e , mass ratio, q , and other properties of the binary star are randomly selected from the following distributions.

Mass ratio, q We have used a ‘flat’ distribution which is uniform in the range $q = 0.2-1$. We did not consider the peaked mass ratio distribution we investigated in Maxted & Jeffries (2005) to be appropriate for the binaries we have discovered in this survey because that distribution is zero for $q < 0.7$ whereas some of the SB1 binaries we have found must have mass ratios $q \lesssim 0.25$. The value of the mass ratio makes little difference to the value of p_{detect} in this range.

Eccentricity, e We have assumed that all binaries with periods less than 10 d have circular orbits (Meibom & Mathieu 2005). Above this period, we assume that the value of e is uniformly distributed in the range $e = 0-e_{\text{max}}$ where $e_{\text{max}} = 0.6$. We have also performed one

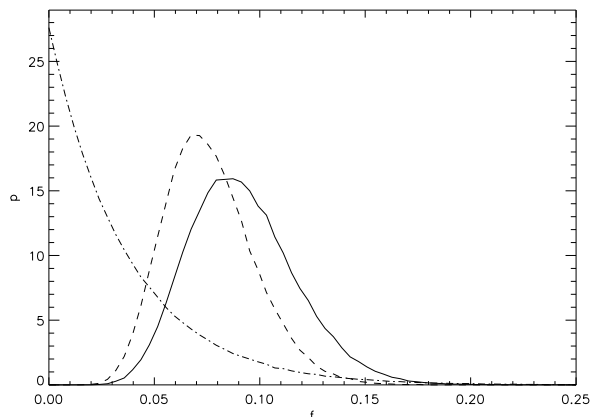


Figure 16. The probability distribution for the binary fraction in our whole sample (dashed line), the ‘bright’ sample (solid lines, mass $> 0.1M_{\odot}$) and the ‘faint’ sample (dashed-dotted line, mass $< 0.1M_{\odot}$).

set of simulations with $e_{\max} = 0$ in order to investigate the effect of assuming that all orbits are circular.

Primary mass, m We have calculated the mass of the primary star based on its I_C magnitude and the models of Baraffe et al. (1998). The mass-magnitude relations shown in Fig. 13 are used to find a primary star mass consistent with the observed magnitude and the mass ratio of the synthetic binary. We allow for an assumed error of 0.03 magnitudes in the observed I_C magnitude. We find that the choice of mass-magnitude relation for each star has a negligible affect on our results. For simplicity, we present the results assuming a distance of 330 parsec and an age of 10 Myr for all stars.

Orbital phase The orbital phase of the binary at the date of the first observation is randomly selected from a uniform distribution in the range 0 to 1.

Longitude of periastron, ω For eccentric binaries, ω is selected from a uniform distribution in the range 0 to 2π .

We have calibrated the extent to which blending between the components reduces the apparent amplitude of the RV variation in a spectroscopic binary. We selected 6 stars with a range of I_C magnitudes that had typical spectra for stars of that magnitude. For each pair of stars we created simulated binary star spectra in which the single star spectra were combined with the appropriate flux ratio for their magnitude difference and a range of velocity offsets between the stars. We then measured the radial velocity of the brighter star in the spectrum in the same way as we did for our actual observations. We used these results to calibrate the difference between the true RV and the apparent RV of the brighter star caused by blending with the spectrum of the fainter star. We used interpolation within the resulting table to adjust the RV of the more massive star in each simulated binary star to account for this blending.

The radial velocities predicted by each trial of the simulation are each perturbed by a random value from a Gaussian distribution with the same standard deviation as the random error of the actual observations. We then estimated the range of inclinations over which the binary would be detected using the same criterion that we applied to our

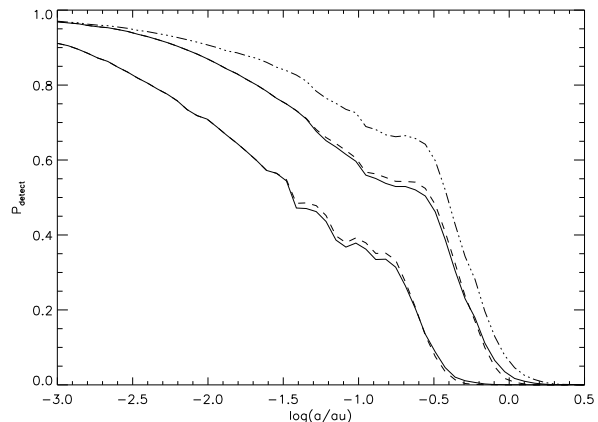


Figure 17. The average detection efficiency for our survey as a function of semi-major axis (a) for the bright sample (upper curves) and the faint sample (lower curves). The solid line corresponds to $e_{\max} = 0.6$, the dashed line to $e_{\max} = 0$ and the dashed-dotted line shows the effect of neglecting blending in the case $e_{\max} = 0.6$ for the bright sample.

actual data. In the absence of blending this is a trivial calculation. In the presence of blending the value of χ^2 may not be a monotonic function of inclination, i . We approximate the true shape of the relation between χ^2 and $\sin i$ using a parabolic fit to the values at $\sin i = 0, 0.5$ and 1 and use this parabolic fit to estimate the range of $\sin i$ values over which the binary would be detected.

The average value of p_{detect} calculated in this way for all the stars in the bright and faint samples are shown as a function of $\log a$ in Fig. 17. From that figure we see that assuming circular orbits does not make a large difference to the value of p_{detect} , but that neglecting blending can lead to an overestimate of the detection efficiency by as much as 15 percent. We can also see that the detection efficiencies calculated above using the RV data of the binaries themselves gives a result consistent with the values of p_{detect} in Fig. 17 if the semi-major axes of these binaries are in the range $-2.5 \lesssim \log(a/au) \lesssim -1.0$. The corresponding range in orbital periods is $0.1 \text{ d} \lesssim P \lesssim 30 \text{ d}$, which is in good agreement with the likely orbital periods of the binaries we have detected.

4.4 Comparison with Kenyon et al. (2005)

We combined our radial velocity data with those of Kenyon et al. (2005) to see if the combined data sets would yield any further spectroscopic binaries. We did not find any new binaries among the 45 stars in common between the two surveys. This is, perhaps, not surprising given the much higher radial velocity accuracy of our data compared to Kenyon et al.. This is as a result of the higher signal-to-noise, higher resolution and superior telluric subtraction achievable with GIRAFFE spectrograph compared with the WYFFOS spectra available to Kenyon et al. The mean difference in the measured radial velocity between the two sets of data is $0.72 \pm 0.44 \text{ km s}^{-1}$.

The star KJN2005 72 (J053739.6–021826) was identified as a possible spectroscopic binary by Kenyon et al.

(2005) based on a RV shift of $35 \pm 4 \text{ km s}^{-1}$ between two spectra obtained on consecutive nights. The radial velocities for this star measured from our data are constant to within a 2 km s^{-1} over a baseline of 63 days. We conclude that the radial velocity shift measured by Kenyon et al. (2005) for this star is likely to be spurious.

Similarly, Kenyon et al. claim a RV shift of $13 \pm 6 \text{ km s}^{-1}$ for the star KJN2005 74 (J053926.8–023656) between two spectra obtained on consecutive nights. We find the RV for this star is constant to within 2 km s^{-1} from 3 spectra with a baseline of 61 days.

Kenyon et al. note that the star KJN2005 46 (J054000.1–025159) appears to be a member based on the presence of the Li I 6707 Å line in the spectrum and the equivalent width of the Na I doublet, but the RV they measure ($17 \pm 3 \text{ km s}^{-1}$) is inconsistent with cluster membership. They suggest that this may be due to this star being spectroscopic binary. However, we find that this star has a mean radial velocity of 30.5 km s^{-1} which is consistent with cluster membership and is constant to within 1 km s^{-1} from 3 spectra with a baseline of 61 days.

In summary, it appears that the radial velocities measured by Kenyon et al. sometimes show spurious shifts of approximately 10 km s^{-1} .

5 DISCUSSION

There are several examples of VLMS and BDs that are clearly spectroscopic binaries. Stassun et al. (2006) measured accurate masses and radii for the brown dwarf pair 2MASS J05352184–0546085 which is an eclipsing spectroscopic binary with an orbital period of 9.8 days and a total mass of $0.088 M_{\odot}$ in the Orion Nebula cluster (ONC). PPl 15 in the Pleiades was the first brown dwarf confirmed by the detection of lithium and is an SB2 spectroscopic binary containing two brown dwarfs with masses of 60–70 Jupiter masses, an orbital period of 5.8 days and an eccentricity of 0.4 (Basri & Martín 1999). There is no large RV survey for spectroscopic binary VLMS and BDs in the Pleiades so we do not know whether PPl 15 is representative of the binary population in this cluster. Similar arguments apply to 2MASS J05352184–0546085 and the ONC. Intriguingly, there is a very well populated binary sequence in the colour-magnitude diagram for the Pleiades (Lodieu et al. 2007), which suggests a binary frequency of 28–44 percent in the $0.075\text{--}0.030 M_{\odot}$ mass range.

Surveys for spectroscopic binaries among late-M and T dwarfs in the field and in nearby clusters have discovered a few other SB2 binaries and several stars that show RV shifts of a few km s^{-1} or less. Basri & Reiners (2006) summarize the results of these surveys and present the results of their own survey of 53 VLMS and BDs. From their own sample they estimate a binary frequency of 11 percent in the separation range 0–6 au. This binary frequency may be consistent with our results for VLM binaries (binary fraction < 7 percent for mass $\lesssim 0.1 M_{\odot}$) if the distribution of a is not strongly biased towards small a . This is reasonable given that none of the binaries detected by Basri & Reiners were SB2 binaries and that the typical radial velocity shifts detected were small (few km s^{-1}).

It is much harder to interpret the results of previous

surveys summarized by Basri & Reiners (2006), not only because of the small number of stars observed but also because there is a bias in these surveys due to preferentially observing brighter stars or imposing a magnitude limit. This tends to increase the number of binaries in these samples, particularly SB2 binaries. Our survey is much less strongly affected by this type of bias. Some SB2 stars will be missing from our sample because they exceed our bright magnitude cut-off. The lack of faint binaries in our sample means there is no compensating gain in SB2 binaries at the faint end of the sample. This bias can only increase the statistical significance of the change in binary properties near $I_C \approx 16.9$ that we have discovered. It is difficult to estimate the compensating bias introduced by excluding stars below the cluster sequence in the I_C v. $R_C - I_C$ colour magnitude diagram but this effect is expected to be small.

It is also harder to characterize the sources of noise in small surveys. This is apparent from the results of Kenyon et al. (2005) in which the few RV shifts they measured of about 10 km s^{-1} were ascribed to binary motion, both by Kenyon et al. and by Maxted & Jeffries (2005). In that case it appears that there is some problem with obtaining reliable RV measurements from spectra affected by telluric absorption with low resolution and low signal-to-noise. A similar problem applies to the interpretation of radial velocity shifts $\lesssim 1 \text{ km s}^{-1}$, even for spectra of the highest quality. At this level, line profile variations due to chromospheric activity and star spots (“jitter”) may become important, but the extent of this effect has not been well characterized. Our survey may also suffer from this problem in the case of some of the SB1 binaries we have detected. For stars with narrow lines and large RV shifts such as J053805.6–024019 this is unlikely to be an issue. For example, Joergens & Mueller (2007) have shown that the star Cha H α 8 is a binary star with an eccentric orbit ($e = 0.49$) and a low mass companion in a wide orbit ($a \approx 1$ au). The semi-amplitude of the orbit is low ($K = 1.6 \text{ km s}^{-1}$) but can be measured reliably because the level of jitter in this young, narrow-lined VLM star is much less than 1 km s^{-1} . It is less certain that stars like J053455.2+100035 with broad spectral lines and small RV shifts are genuine spectroscopic binaries. One mitigating factor in our survey is that there are several other stars in our survey with broad lines that are not detected as binary stars, so it does appear that we can measure radial velocities accurate to about 1 km s^{-1} in this type of star. Nevertheless, it remains to be established that any of the single-lined stars showing RV shifts from this survey, the survey by Basri & Reiners (2006) or the survey by Guenther & Wuchterl 2003 are genuine SB1 spectroscopic binaries with Keplerian orbits.

Note, however, that the statistical significance of the change in binary properties for very low mass stars in this survey we have noted remains high (> 97 percent) even if we consider only the SB2 binaries.

It is harder to detect binary stars among rapidly rotating stars because the RV measurements from broader CCFs is less precise than for narrow CCFs. This does not affect our conclusion that there is a change in binary properties for very low mass stars compared to low-mass stars because rapidly rotating stars are evenly distributed in magnitude within our sample and the standard errors of the radial ve-

locities we assign to these stars accurately accounts for the effects of line broadening.

A rapid change in close binary fraction at a given magnitude is only approximation to what is, in reality, likely to be a gradual change in binary properties with mass. We do not have enough data to be able to say with any accuracy at which mass this change occurs or whether the change occurs over a small or large range of masses. This is why we have presented results with the sample divided into bright and faint sub-samples at $I_C = 16.9$, a magnitude that corresponds to the commonly accepted dividing line between VLMS/BDs and low-mass stars at $0.1M_\odot$.

With only 11 binaries and 3 or 4 RV measurements per star we cannot say a great deal about the distribution of the binaries properties in low mass star with the data available so far. However, we do have estimates of the mass ratio in these binaries. The mass ratio is clearly $q \approx 1$ in the case of the SB2 binaries with nearly equal components (“twins”). For the stars where no companion is visible and the spectral lines are narrow we estimate that the companion is likely to be at least 2.5 magnitudes fainter than the primary and so $q \lesssim 0.25$. The star J053455.2+100035 lies somewhere between these extremes. The overall picture, then, is of a peak in the mass ratio distribution near $q = 1$ due to twins overlaid on a broader distribution increasing towards small values of q . This is qualitatively similar to the mass ratio distribution found for low mass Population I stars by Goldberg et al. (2003) and the mass ratio distribution for solar-type stars measured by Halbwachs et al. (2003) for solar type stars in the solar neighbourhood, Pleiades and Praesepe. Goldberg et al. find that the peak in the q distribution due to twins is not present for Pop I binaries more massive than $0.67M_\odot$ or for halo stars. Halbwachs et al. find that the peak for $q > 0.8$ gradually decreases when long-period binaries are considered.

We have estimated the number of binaries we would detect if the stars brighter than $I_C=16.9$ (mass $\approx 0.1M_\odot$) in our sample have the same binary frequency and orbital period distribution as nearby M-dwarfs. We used the detection efficiency for each star as a function of $\log P$ convolved with the Gaussian distribution for $\log P$ from Duquennoy & Mayor (1991) together with the binary fraction for M-dwarfs of 42 percent from Fischer & Marcy (1992) to find that we would have detected 6.5 spectroscopic binaries an average in our survey given these assumptions. At face value, this suggests that the frequency of short period binaries among low mass stars in λ Ori and σ Ori is slightly larger to that for nearby M-dwarfs. However, the assumption that the distribution of $\log P$ established by Duquennoy & Mayor for solar-type stars is appropriate for low mass stars may not be correct. Fischer & Marcy find that the period distribution for M-dwarfs binaries is similar to that for solar type stars but there is only one short period M-dwarf binary in the sample so the period distribution is poorly characterized at the short period end. Duquennoy & Mayor note that Griffin (1985) measured a much higher frequency of short period binaries for solar type stars in the Hyades than is seen in their field star sample. The same effect was seen to a lesser extent by Halbwachs et al., so both environment and primary mass may be important factors in determining the frequency of short period binaries in our sample. We do not have suffi-

cient data in our survey to measure the orbital periods and semi-amplitudes of the spectroscopic binaries we have detected.

Given the uncertainty in the orbital period distribution of low mass stars it would clearly be worthwhile to obtain complete orbits for the binary stars we have identified. The maximum separations of the lines observed in the SB2 binaries and the timescale and amplitude of the RV variations for the SB1 binary stars suggest that the orbital periods of these binaries are likely to be in the range from several hours to several days. An anonymous referee has raised the possibility that the difference in binary fraction we have observed in the bright and faint samples is due to a distribution of $\log a$ strongly biased towards $\log(a/au) \gtrsim -0.5$. It can be seen from Fig. 17 that we have almost no sensitivity to binaries within the faint sample but good sensitivity to binaries within the bright sample in this $\log a$ range. In principle, it may be possible to find a distribution of $\log a$ that can explain the numbers of binaries detected in the bright and faint samples for a single value of the binary fraction. However, such a distribution would be incompatible with the observation that several of the binaries we have discovered have short orbital periods corresponding to values of $\log(a/au) \ll -0.5$. If it were the case that the binaries we have detected are biased towards $\log(a/au) \gtrsim -0.5$ then the values of $f_{\text{empirical}}$ we calculated for stars in the faint sample would have been very small. In this case, the probability distribution for the binary fraction calculated in section 4.2 would have been consistent with the hypothesis $f_{\text{faint}} = f_{\text{bright}}$. In fact, this hypothesis can be rejected with 90 percent confidence, so the binaries we have detected are not biased towards $\log(a/au) \gtrsim -0.5$.

The lack of binaries in our sample with masses $\lesssim 0.1M_\odot$ is consistent with the overall picture established from existing surveys that the binary fraction for VLMS and BDs across the full range of orbital separations is 20–25 percent (Allen 2007; Basri & Reiners 2006). However, the binary properties for VLMS and BDs is poorly characterized in the range $a \lesssim 2$ au that is below the detection limits of high angular resolution imaging. Some VLMS and BDs show apparent RV shifts comparable to the orbital speeds expected at these separations, and a complete spectroscopic orbits has now been published for one such star (Cha H α 8, Joergens & Mueller 2007). It is still possible given all the observations to-date that there is a large population of VLMS/BD binaries with $a \approx 1$ au. If such a population exists then it may be possible to reconcile the binary fraction in existing surveys with the high binary fraction inferred for the Pleiades by Lodieu et al. (2007).

The spectra we have used for this study were obtained with the aim of measuring the binary properties of the low mass stars and brown dwarfs in the λ Ori and σ Ori clusters but there is clearly useful information to be obtained about the properties of the clusters themselves from the spectra we have obtained. For example, the distribution of EW(NaI) shown in Fig. 12 clearly shows that the stars in λ Ori have higher surface gravities on average than stars in Group 2 of the σ Ori cluster. This shows that the λ Ori cluster is older than the Group 2 of the σ Ori cluster and, perhaps, has a similar age to Group 1 of the σ Ori cluster. This is in general agreement with the ages we have adopted for these

populations. A more detailed analysis is beyond the scope of this paper.

6 CONCLUSIONS

We have conducted a large radial velocity survey for spectroscopic binary stars among low mass stars and brown dwarfs in the young clusters around λ Ori and σ Ori. We have identified 196 members of these clusters based on their radial velocity and spectral type. Of these, 6 are SB2 binaries and 6 are SB1 binaries. All the spectroscopic binaries we have detected are brighter than $I_C=16.6$ (mass $\approx 0.12M_\odot$). We conclude that the frequency of spectroscopic binaries in these clusters among very low mass stars (mass $< 0.1M_\odot$) and brown dwarfs is significantly lower (< 7.5 percent) than that for more massive stars (9 ± 2 percent). The change in binary properties with mass that we have discovered may be due to a change in the total binary frequency with mass or a change in the period distribution of the binaries with mass or both.

The number of SB2 binaries in this sample suggests there may be a peak in the mass ratio distribution for spectroscopic binaries in these clusters near $q \approx 1$. There is also clear evidence from the properties of the SB1 binaries that the mass ratio distribution for spectroscopic binaries in these clusters is broad, extending down to $q \approx 0.25$.

ACKNOWLEDGMENTS

Based on observations collected at the European Southern Observatory, Chile (Programme ID: 076.C_145). RJJ was supported by a Nuffield Undergraduate Research Bursary. This research is partially funded by a Science & Technology Facilities Council research grant (formerly PPARC). We thank the referee for comments that helped to improve the clarity of this paper.

REFERENCES

- Allen P. R., 2007, *ApJ*, 668, 492
 Baraffe I., Chabrier G., Allard F., Hauschildt P. H., 1998, *A&A*, 337, 403
 Barrado y Navascués D., Béjar V. J. S., Mundt R., Martín E. L., Rebolo R., Zapatero Osorio M. R., Bailer-Jones C. A. L., 2003, *A&A*, 404, 171
 Barrado y Navascués D., Stauffer J. R., Bouvier J., Jayawardhana R., Cuillandre J.-C., 2004, *ApJ*, 610, 1064
 Basri G., Martín E. L., 1999, *AJ*, 118, 2460
 Basri G., Reiners A., 2006, *AJ*, 132, 663
 Béjar V. J. S., Zapatero Osorio M. R., Rebolo R., 2004, *Astronomische Nachrichten*, 325, 705
 Blecha A., Cayatte V., North P., Royer F., Simond G., 2000, in Iye M., Moorwood A. F., eds, *Proc. SPIE Vol. 4008*, p. 467-474, *Optical and IR Telescope Instrumentation and Detectors*, Masanori Iye; Alan F. Moorwood; Eds. Vol. 4008 of Presented at the Society of Photo-Optical Instrumentation Engineers (SPIE) Conference, Data-reduction software for GIRAFFE, the VLT medium-resolution multi-object fiber-fed spectrograph. pp 467–474
 Bouy H., Brandner W., Martín E. L., Delfosse X., Allard F., Basri G., 2003, *AJ*, 126, 1526
 Burgasser A. J., Reid I. N., Siegler N., Close L., Allen P., Lowrance P., Gizis J., 2007, in Reipurth B., Jewitt D., Keil K., eds, *Protostars and Planets V Not Alone: Tracing the Origins of Very-Low-Mass Stars and Brown Dwarfs Through Multiplicity Studies*. pp 427–441
 Close L. M., Siegler N., Freed M., Biller B., 2003, *ApJ*, 587, 407
 Dekker H., D’Odorico S., Kaufer A., Delabre B., Kotzowski H., 2000, in Iye M., Moorwood A. F., eds, *Proc. SPIE Vol. 4008*, p. 534-545, *Optical and IR Telescope Instrumentation and Detectors*, Masanori Iye; Alan F. Moorwood; Eds. Vol. 4008 of Presented at the Society of Photo-Optical Instrumentation Engineers (SPIE) Conference, Design, construction, and performance of UVES, the echelle spectrograph for the UT2 Kueyen Telescope at the ESO Paranal Observatory. pp 534–545
 Duquennoy A., Mayor M., 1991, *A&A*, 248, 485
 Fischer D. A., Marcy G. W., 1992, *ApJ*, 396, 178
 Goldberg D., Mazeh T., Latham D. W., 2003, *ApJ*, 591, 397
 Griffin R. F., 1985, in Eggleton P. P., Pringle J. E., eds, *NATO ASIC Proc. 150: Interacting Binaries The distributions of periods and amplitudes of late-type spectroscopic binaries*. pp 1–12
 Guenther E. W., Wuchterl G., 2003, *A&A*, 401, 677
 Halbwachs J. L., Mayor M., Udry S., Arenou F., 2003, *A&A*, 397, 159
 Hanuschik R. W., 2003, *A&A*, 407, 1157
 Horne K., 1986, *PASP*, 98, 609
 Jeffries R. D., Maxted P. F. L., Oliveira J. M., Naylor T., 2006, *MNRAS*, 371, L6
 Joergens V., Mueller A., 2007, *ArXiv e-prints*, 710
 Kenyon M. J., Jeffries R. D., Naylor T., Oliveira J. M., Maxted P. F. L., 2005, *MNRAS*, 356, 89
 Kraus A. L., White R. J., Hillenbrand L. A., 2005, *ApJ*, 633, 452
 Kurosawa R., Harries T. J., Littlefair S. P., 2006, *MNRAS*, 372, 1879
 Lodieu N., Dobbie P. D., Deacon N. R., Hodgkin S. T., Hambly N. C., Jameson R. F., 2007, *ArXiv e-prints*, 706
 Maxted P. F. L., Jeffries R. D., 2005, *MNRAS*, 362, L45
 Mayne N. J., Naylor T., Littlefair S. P., Saunders E. S., Jeffries R. D., 2007, *MNRAS*, 375, 1220
 Meibom S., Mathieu R. D., 2005, *ApJ*, 620, 970
 Mohanty S., Basri G., Jayawardhana R., Allard F., Hauschildt P., Ardila D., 2004, *ApJ*, 609, 854
 Nicholls R. W., 1988, *Journal of Quantitative Spectroscopy and Radiative Transfer*, 40, 275
 Padoan P., Nordlund Å., 2004, *ApJ*, 617, 559
 Pasquini L., Avila G., Blecha A., Cacciari C., Cayatte V., Colless M., et al. 2002, *The Messenger*, 110, 1
 Pasquini L., Castillo R., Dekker H., Hanuschik R., Kaufer A., Modigliani A., Palsa R., Primas F., Scarpa R., Smoker J., Wolff B., 2004, in Moorwood A. F. M., Iye M., eds, *Ground-based Instrumentation for Astronomy*. Edited by Alan F. M. Moorwood and Iye Masanori. *Proceedings of the SPIE*, Volume 5492, pp. 136-147 (2004). Vol. 5492 of Presented at the Society of Photo-Optical Instrumentation Engineers (SPIE) Conference, Performance of FLAMES at the VLT: one year of operation. pp 136–147

- Reipurth B., Clarke C., 2001, *AJ*, 122, 432
- Rothman L. S., Jacquemart D., Barbe A., Benner D. C., Birk M., Brown L. R., et al. 2005, *Journal of Quantitative Spectroscopy and Radiative Transfer*, 96, 139
- Schiavon R. P., Barbuy B., Rossi S. C. F., Milone A., 1997, *ApJ*, 479, 902
- Stassun K. G., Mathieu R. D., Valenti J. A., 2006, *Nature*, 440, 311
- Topping J., 1962, *Errors of Observation and Their Treatment*. Chapman & Hall
- Whitworth A. P., Stamatellos D., 2006, *A&A*, 458, 817
- Whitworth A. P., Zinnecker H., 2004, *A&A*, 427, 299

This figure "SOri_1_R1_tellfit.gif" is available in "gif" format from:

<http://arxiv.org/ps/0801.3595v1>

This figure "example_spectra.gif" is available in "gif" format from:

<http://arxiv.org/ps/0801.3595v1>

This figure "sori_ri.gif" is available in "gif" format from:

<http://arxiv.org/ps/0801.3595v1>